

# An Optical Neuromorphic Sensor with High Uniformity and High Linearity for Indoor Visible Light Localization

Shuai Zhong,\* Jiachao Zhou, Fangwen Yu, Mingkun Xu, Yishu Zhang,\* Bin Yu, and Rong Zhao\*

The visible light localization system holds great promise as a highly accurate indoor positioning method. However, it still suffers deficiencies including high latency and power consumption, and large area cost. To address these issues, a high energy efficient spiking localization system inspired by the biological spatial representation system is presented. This system utilizes an optical neuromorphic sensor, consisting of a compact NbO<sub>x</sub>-based threshold switching memristor and a photoresistor. The key lies in the system's ability to convert analog light information into electrical spikes, resembling the behavior of sensory neurons, which enables the encoding of light illuminance through spiking frequency. Consequently, the system achieves high uniformity, high linearity ( $\approx 10\%$ ), and high sensitivity ( $\approx 1.1 \text{ kHz Lux}^{-1}$  and  $\approx 72.7 \text{ kHz cm}^{-1}$  for light illuminance and distance detection, respectively), indicating its potential suitability for visible light localizations. By leveraging a spiking neural network classifier, the system successfully distinguishes locations with different illuminances. After 150 epochs, it achieves an accuracy of 97%, showcasing the feasibility of using the spiking localization system in real-world applications. The approach of spike-based light positioning is a leap forward toward the development of future compact, highly energy-efficient visible light localization systems.

such as museum, hospital, and shopping mall.<sup>[1,2]</sup> These services not only familiarize users with their surroundings immediately, but also enable the delivery of accurate commercial services when combined with other technologies. While Global Positioning System is the dominant approach for localization with merits of wide coverage, its signals get attenuated by indoor structures like walls and ceilings, and multipath distortion in indoor settings,<sup>[3]</sup> which impacts accuracy and stability of positioning. This limitation calls for alternative solutions, and considerable efforts have been devoted to developing indoor localization strategies using wireless communication methods, for example, ultra-wideband, radio frequency identification, Wi-Fi signal, Bluetooth, or other methods.<sup>[4-6]</sup> However, these methods have shortcomings in terms of accuracy, cost, and low bandwidth.

To overcome these challenges, a promising indoor localization system based on visible light communication

(VLC) has been introduced due to the merits of low cost, high positioning precision, wide bandwidth, and long service life.<sup>[7,8]</sup> The visible light localization system (VLLS) generally includes

## 1. Introduction

Indoor location-based services (ILBS) have garnered increasing interest because of their wide application in various scenarios,

S. Zhong, M. Xu  
Guangdong Institute of Intelligence Science and Technology  
Hengqin, Zhuhai 519031, China  
E-mail: zhongshuai@gdiist.cn  
S. Zhong, F. Yu, R. Zhao  
Department of Precision Instruments  
Tsinghua University  
Beijing 100084, China  
E-mail: r\_zhao@mail.tsinghua.edu.cn

J. Zhou, Y. Zhang, B. Yu  
School of Micro-Nano Electronics  
Zhejiang University  
Hangzhou 310027, China  
E-mail: zhangyishu@zju.edu.cn

J. Zhou, Y. Zhang, B. Yu  
ZJU-Hangzhou Global Scientific and Technological Innovation Center  
College of Micro-Nano Electronics  
Zhejiang University  
Hangzhou 311200, China

R. Zhao  
Innovation Center for Future Chip  
Tsinghua University  
Beijing 100084, China

R. Zhao  
Center for Brain-Inspired Computing Research  
Tsinghua University  
Beijing 100084, China

 The ORCID identification number(s) for the author(s) of this article can be found under <https://doi.org/10.1002/adsr.202300197>

© 2024 The Authors. Advanced Sensor Research published by Wiley-VCH GmbH. This is an open access article under the terms of the [Creative Commons Attribution](#) License, which permits use, distribution and reproduction in any medium, provided the original work is properly cited.

DOI: 10.1002/adsr.202300197

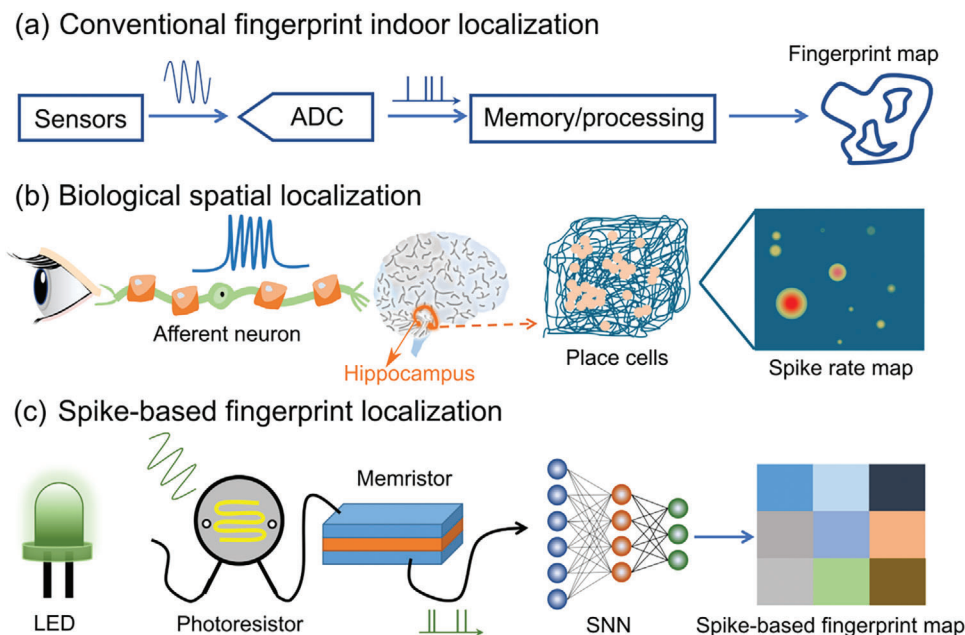


**Figure 1.** Conventional localization system, biological spatial localization system and our bio-inspired proposed localization system. a) For conventional localization system, external stimuli are received by the sensor and transduced into spikes by the analog-to-digital converter module. Then, a fingerprint map is obtained after data processing through memory/processors. b) Light information is first perceived by the eyes in biological spatial localization system and then converted into spikes via afferent neuron. These spikes will be sent to hippocampus to activate the place cells. The spike frequency of the targeted area is higher compare to that of other areas. c) Our proposed VLLS consists of an optical neuromorphic sensor and a SNN classifier. The optical neuromorphic sensor receives the light information and transduces it into electrical spikes. The output spikes are subsequently fed into the SNN for recognition.

two main components: transmitter and receiver. The transmitter serves as the light source with or without modulation, while the receiver comprises photodiodes for light collection and an analog-to-digital converter for signal conversion for further processing by conventional computer.<sup>[9]</sup> However, current signal conversion circuits hold some drawbacks, such as large hardware area, high power consumption and latency. Additionally, massive data processing through the von Neumann architecture inevitably increases power consumption and reduces computing efficiency because of the well-known “memory wall”.<sup>[10,11]</sup> Therefore, there is a pressing need to develop VLLS solutions that process data in a more energy-efficient way, especially in future data-intensive circumstances.

Designing efficient VLLS can take inspiration from the biological spatial representation system (BSRS).<sup>[12,13]</sup> The BSRS processes external stimuli by converting them into electrical spikes, which are then transmitted to the hippocampus for spatial memory and representation.<sup>[14]</sup> Specifically, receptors encode multimode sensory cues into spikes,<sup>[15]</sup> serving as drivers to activate hippocampal neurons, known as place cells.<sup>[16,17]</sup> Different place cells fire when the person locates in different positions, enabling humans to navigate their environment effectively. Such highly parallel and energy efficient system outperforms current positioning technologies in processing intensive real-time data, especially in complex surroundings. The potential to build an energy-efficient VLLS system arises from the insights of the BSRS. Although previous works have explored artificial sensory system,<sup>[18–20]</sup> artificial afferent/efferent nerve,<sup>[21–26]</sup> and elec-

tronic skin,<sup>[27–29]</sup> a bio-inspired artificial VLLS system with high energy efficiency remains elusive.

Here, we report a spike-based VLLS system comprising an optical neuromorphic sensor and a spiking neural network (SNN). The optical neuromorphic sensor, built on an NbO<sub>x</sub>-based threshold switching (TS) memristor and a photoresistor, receives the external light information and converts them into electrical spikes. The spike frequency is found to correlate significantly with illuminance or distance, making it suitable for position encoding. Notably, the optical neuromorphic sensor exhibits competitive parameters, including uniformity, linearity (10%), and sensitivity (1.1 kHz Lux<sup>-1</sup> or 72.7 kHz cm<sup>-1</sup>). To validate the system’s effectiveness, we coupled optical neuromorphic sensor with an SNN classifier. The system successfully discriminated positions with different illuminance levels, achieving 97% accuracy after 150 epochs. This work showcases the great potential of optical neuromorphic sensors for high energy-efficient VLLS and serves as a driving force for the development of ILBS.

## 2. Results and Discussion

**Figure 1a** illustrates the workflow of the conventional VLLS. The process involves signal transduction and processing, leading to the creation of a fingerprint map that reflects the real environment. The fingerprint technique, widely-used in VLLS, labels locations based on distinct features or characteristics of signals.<sup>[30]</sup> These features can include time difference of arrival, time of arrival, angle of arrive, angle difference of arrival, and re-

ceived signal strength (RSS). Each specific feature corresponds to a particular position in the environment. The fingerprint localization process comprises two phases: offline signal collection and online positioning. In the offline stage, light signals from various positions are received, processed, and stored, resulting in the creation of a fingerprint map. In the online stage, localization is performed by comparing the post-processed signal with the data in the fingerprint map. Figure 1b depicts the physiological path of the BSRS, where various sensory signals are transmitted to the hippocampus in a spiking fashion and then fused to activate place cells. Utilizing spike-based processing and computation, the BSRS operates with high energy efficiency. By recording the neural behavior of place cells, a cognitive map is obtained, showing the relationship between cell firing rates and positions. It is important to note that while a place cell may exhibit similar firing behavior in different surroundings, the highly sensitive cognitive maps vary from one location to another.<sup>[16]</sup> Figure 1c presents our experimental design of a high energy efficient VLLS that is akin to the BSRS. In this design, a light emitting diode (LED) serves as the stimulus source, a photoresistor acts as the receptor, a TS memristor functions as the analog-to-spike transducer, and a SNN is used to process the converted spike signals. Through investigating the spiking behavior induced by different light intensities at different positions, an offline spike-based fingerprint map is accomplished. The online SNN enables precise position identification by sorting the spike signals.

Due to its high scalability and easy integration, it has been reported that memristors can be used for neuromorphic sensors. However, the features such as high uniformity, high linearity—all of which are essential for a neuromorphic sensor—is ignored. Evidently, all these properties are strongly correlated to the performance of memristor, which we first optimized in terms of uniformity, power consumption and compatible with external sensor via structure and material engineering. Figure 2a presents the device structure of the memristor, featuring a dielectric NbO<sub>x</sub> layer sandwiched between Pt electrodes. To analyze the elemental distribution and cross-sectional properties, energy-dispersive X-ray spectroscopy (Figure S1, Supporting Information) was conducted. The electrical measurement of the memristor is depicted in Figure 2b. An abrupt transition from a high resistance state (HRS) to a low resistance state (LRS) occurs when the applied voltage exceeds the threshold voltage ( $V_{th}$ ,  $\approx 1.77$  V). Upon the voltage dropping below the holding voltage ( $V_{hold}$ ,  $\approx 1.63$  V), the memristor automatically returns to the HRS. A compliance current ( $I_{cc}$ ) of 0.7 mA is clamped to prevent the device's hard breakdown. The memristor maintains its threshold switching properties after 100 cycles, showing good repeatability. The electrical uniformity of the device is also commendable, with a coefficient of variation (CV) of 0.54% for  $V_{th}$  and 0.59% for  $V_{hold}$  (Figure S2, Supporting Information), which is rival to previous reports, as shown in Table S1 (Supporting Information). Here, the CV is defined as  $CV = \sigma/\mu$ , where  $\sigma$  is the standard deviation and  $\mu$  is the mean value. The TS phenomenon of the NbO<sub>x</sub> memristor can be well elucidated using the Mott transition.<sup>[31,32]</sup> A detailed explanation can be found in Figure S3 (Supporting Information). The high uniformity can be probably ascribed to the formation of stable conducting filament during threshold switching due to the structure and stoichiometry engineering. Additionally, the switch speed of the TS memristor is measured, with switch-

on and switch-off speed is  $\approx 200$  ns at 2 V and  $\approx 80$  ns at 1.4 V, respectively, in line with the  $V_{th}$  and  $V_{hold}$  values observed in DC testing (Figure S4, Supporting Information).

By employing the TS memristor in conjunction with an external resistor, a transducer that can convert analog signals to spikes is fabricated, as displayed in Figure 2c. To ensure proper functionality, the resistor value should fall within the range of  $R_{LRS}$  and  $R_{HRS}$  ( $R_{LRS} < R_{ext} < R_{HRS}$ ). At the initial stage, since the  $R_{HRS}$  is larger than the  $R_{ext}$ , most of the applied voltage drops across the memristor, resulting in the charging of capacitor. When the memristor switches from HRS to LRS, as the  $R_{LRS}$  is smaller than the  $R_{ext}$ , the applied voltage on the device decreases immediately, initiating a discharge of the capacitor. The device returns to HRS once the voltage drops below  $V_{th}$ , starting a new charge-discharge cycle. Briefly, the following two equations must be satisfied:

$$\frac{R_{HRS} \times V_{applied}}{R_{HRS} + R_{ext}} \geq V_{th} \quad (1)$$

$$\frac{R_{LRS} \times V_{applied}}{R_{LRS} + R_{ext}} \leq V_{hold} \quad (2)$$

Figure 2d illustrates a typical dynamic behavior of the transducer. Triggered by a voltage pulse, a current spike train is generated. The frequency of these spikes is expected to be governed by the external resistor (see Figure 2e; Figure S5, Supporting Information). There exists an inverse relationship between the resistor and spike frequency: as the  $R_{ext}$  increases, the spike frequency decreases. Besides, the spike frequency is also affected by the voltage pulse amplitude (see Figure 2f). The larger pulse amplitude produces a higher spike frequency. These attributes are closely related to the variations in charging/discharging time, which are strikingly dependent on the external resistor, applied voltage, and capacitor. The ideal spike frequency can be theoretically determined by the following equation:<sup>[33]</sup>

$$f = \frac{1}{R_{ext} C \log\left(\frac{V_{hold} - V}{V_{th} - V}\right)} \quad (3)$$

where  $C$  is the total capacitor,  $R_{ext}$  is the external resistor and  $V$  is the applied voltage.

In addition, the range of applied voltage is primarily determined by the connected resistor, as demonstrated in Figure S6 (Supporting Information). When using a smaller resistor, the voltage required to trigger spikes decreases, aligning well with the voltage divider rule. Ensuring the uniformity of the transducer is of significant concern. Figure 2g demonstrates the repeatable spiking behavior under the same pulse amplitude, and magnified curves of specific cycles are manifested in Figure 2h. It can be found that no obvious degradation is detected, indicating its robustness. The effect of pulse amplitude on the spiking uniformity is further investigated. The device exhibits excellent repeatability under various voltages (see Figure 2i; Figure S7, Supporting Information). These results verify that the TS memristor-based transducer with high uniformity and reliability is a promising candidate for building neuromorphic sensors capable of sensing stimuli and converting signals.

The VLLS is responsible for sensing visible light and converting it to spikes. To achieve this, we have replaced the resistor

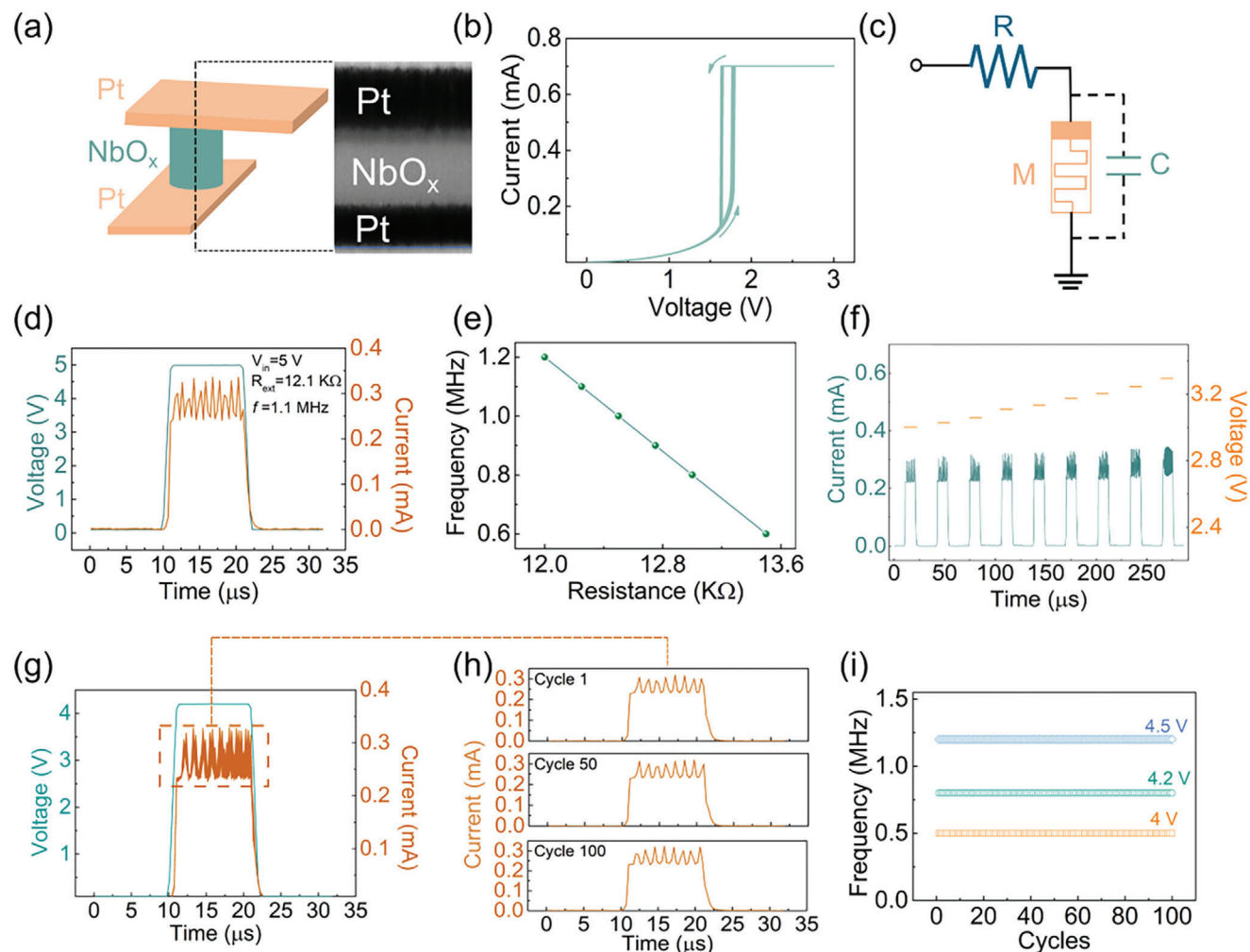


**Figure 2.** Electrical investigation of NbO<sub>x</sub>-based TS memristor and the transducer. a) Schematic of the device structure and its transmission electron microscope (TEM) image. b) DC sweeping of device with 100 cycles. c) Illustration of designed circuit to implement the spiking generation. d) Spiking behavior under certain series resistance and applied voltage. e) Spike frequency modulation as a function of series resistance. f) Effect of the applied voltage on the spike frequency when the series resistance is constant. g) Uniformity examination of the spike performance. After 100 tests, the spike behavior is repeatable, indicating the reliability of the system. h) A magnified spike curve of cycle 1, cycle 50 and cycle 100. i) Uniformity examination of the spike performance under different applied voltages, further suggesting its uniform electrical performance.

with a photoresistor, which allows modulation of resistance based on the light illuminance, thus creating an optical neuromorphic sensor (Figure S8, Supporting Information). As previously mentioned, the change of resistance leads to variations of spike frequency, indicating that spike behavior is regulated by illuminance when a photoresistor is used. Figure 3a shows the relationship between spike frequency and applied voltage under different illuminances of daylight. When illuminance is constant, spike frequency is found to be proportional to the applied voltage, which agrees with the trend illustrated in Figure 2. An important observation is that higher illuminance results in a lower threshold voltage required to trigger spikes, owing to the photoresistor's lower resistance under brighter conditions. These characteristics make the optical neuromorphic sensor promising for illuminance differentiation. VLC-based RSS is a commonly used for ILBS by estimating the distance between the light source and positions. The emitted light strength experiences attenuation with increasing

distance, and light reflection is not considered in this method. Therefore, location identification is achieved by examining the light strength. Our proposed optical neuromorphic sensor can effectively distinguish light signals and convert them to spikes, enabling location differentiation. As illustrated in Figure 3b, position "A" and position "B" are two spots located in the area that illuminance is unevenly distributed, which delineates the illuminance distribution shaped by the space design and layout in real scene. To discriminate, the spiking dynamics of the optical neuromorphic sensor at each point is investigated, as shown in Figure 3c. It is obvious that under the same applied voltage, the spike frequency and amplitude of position "A" are higher than that of position "B". By analyzing these spike signals, the positions "A" and "B" are distinctly separated. In order to make this phenomenon more evident, a Fast Fourier Transform (FFT), which converts a signal from its original domain, such as time or space, into a representation in the frequency domain, was further conducted

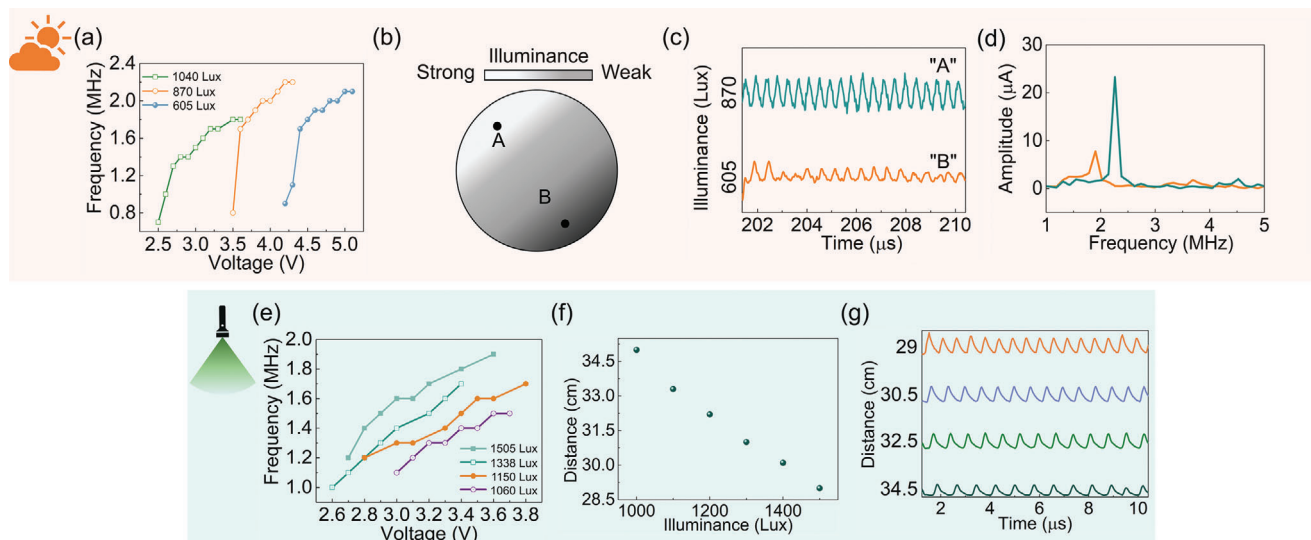


**Figure 3.** Transduction performance of optical neuromorphic sensor. a) Output spike frequency of optical neuromorphic sensor as a function of applied voltage under various illuminance conditions of natural light. b) Schematic of the situation where optical neuromorphic sensor can be used for position classification. c) Spiking behavior of optical neuromorphic sensor when placed at two locations with different illuminances. For the positions that receive diverse illuminances, the differentiation is feasible according to the output spiking dynamics of optical neuromorphic sensor. d) Fast Fourier Transform spectra of spike signal presented in Figure 3c. It can be easily found that the output spikes at two locations with various illuminances pose quite different spike frequency and amplitude. e) Output spike frequency of optical neuromorphic sensor as a function of applied voltage under various illuminance conditions of monochromatic green light. f) Impact of distance between green light source and optical neuromorphic sensor on the illuminance it receives. g) Spiking behavior of optical neuromorphic sensor at four positions with varied distances from the light source.

(Figure 3d). It is apparent that the frequency peaks are well separated, indicating that it is feasible to discriminate positions with distinct light intensities through analyzing the collected spikes. Currently, the VLLS are equipped with LEDs; thus, we further examine the spike performance of the optical neuromorphic sensor under green LEDs (Figure 3e). The illuminance of the light is controlled by tuning light focusing while the distance between the light source and the photoresistor remains fixed (Figure S9). Here, the LED and the photoresistor are on the vertical line. Similar tendency is discerned with that under daylight, although there is significant diversity in the generated spike frequencies. This difference is attributed to the varying absorption efficiency of the photoresistor for daylight and monochrome green light. To incorporate position information, the illuminance is modified by altering the distance between the LED and photoresistor. The illuminance becomes weaker as the distance increases, as demonstrated in Figure 3f, suggesting that distance can be inferred from illuminance, and hence, it can also be represented by the spikes. We then evaluate the spiking behavior at different distances via the optical neuromorphic sensor. Figure 3g presents the spike frequency of optical neuromorphic sensor at distance of 34.5, 32.5, 30.5, 29 cm, respectively. Notably, decreasing the distance will increase the output spiking frequency since short distance signifies higher illuminance, which lowers the resistance of photoresistor and makes the optical neuromorphic sensor generate higher spike frequency. These results demonstrate that analyzing the spiking performance allows recognition of different locations with varying illuminance levels.

In this study, we assess the sensing properties of the optical neuromorphic sensor, focusing on its sensitivity, uniformity, linearity, and power consumption. Sensitivity, denoted as  $S = \Delta f / \Delta v$ ,

measures the change of spiking frequency ( $\Delta f$ ) relative to variations in input variables ( $\Delta v$ ). A higher sensitivity is desirable for a sensor, and we achieve sensitivities of  $1.1 \text{ kHz Lux}^{-1}$  and  $72.7 \text{ kHz cm}^{-1}$  for illuminance and distance inputs, respectively. These values far exceed those reported in previous studies.<sup>[22,26]</sup> Notably, the sensitivity of the optical neuromorphic sensor relies heavily on the applied voltage and can be further improved by tuning the performance of the TS memristor and photoresistor (Figure S10, Supporting Information). It is well known that the uniformity governs the signal encoding accuracy and affects the complexity of peripheral circuit design. The results of uniformity examination of our optical neuromorphic sensor in under natural and green light conditions are shown in Figure 4a,b. Good consistency of spike frequency was maintained for the same light intensity during 100 cycles, indicating robust light encoding capability. Linearity and power consumption, two other crucial properties of neuromorphic sensor, are also evaluated. The linearity of neuromorphic sensor describes how closely the actual spike output aligns with the ideal spike output. While an ideal spike output would form a straight line, various factors, such as material defects or device variations, make achieving perfect linearity challenging in practical applications. The linearity is often expressed as the percentage of nonlinearity, which can be characterized as

$$\text{Nonlinearity} = \frac{D_{\text{out(max)}}}{\text{Out}_{f,s}} \times 100\% \quad (4)$$

where  $D_{\text{out(max)}}$  is the maximum output deviation of spikes, and  $\text{Out}_{f,s}$  is the full-scale output of spikes, as illustrated in Figure 4c. By adopting the end-point linearity approach and establishing the relationship between spike frequency and illuminance,

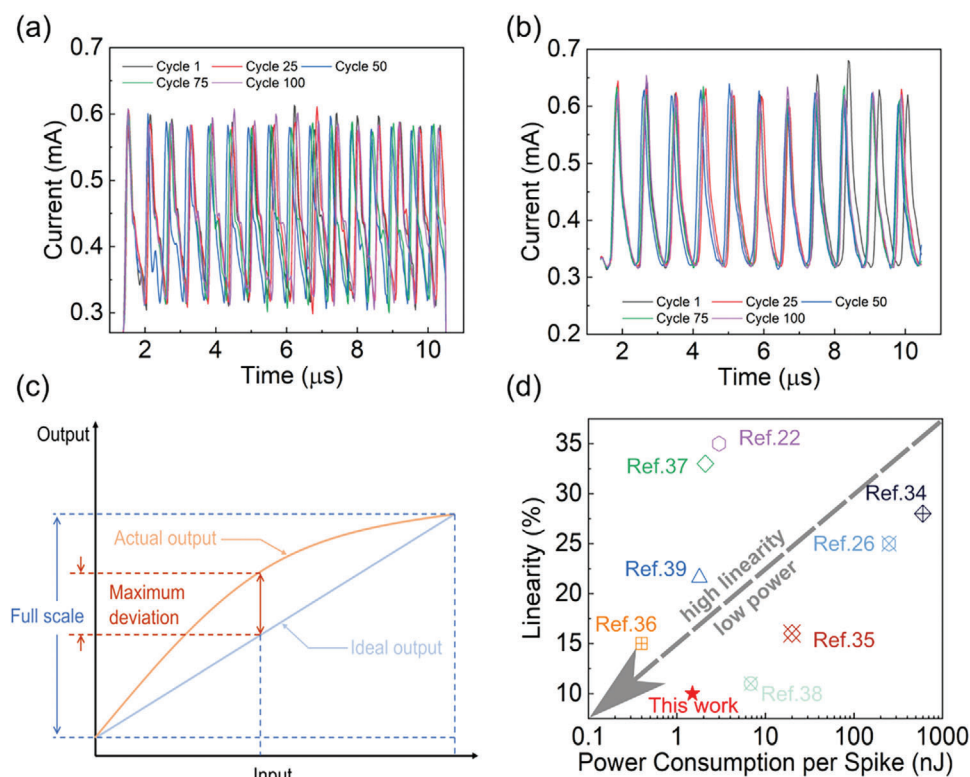


**Figure 4.** Performance evaluation of optical neuromorphic sensor. Uniformity investigation of optical neuromorphic sensor under a) natural light and b) green light. c) Schematic of linearity evaluation. The linearity is determined by the maximum output deviation and full-scale output of spikes. d) Power consumption and linearity comparison. The power consumption is calculated by power consumption of the applied pulse and the number of generated spikes and it can be found that our optical neuromorphic sensor shows competitive with pervious works.

our optical neuromorphic sensor exhibits a linearity of  $\approx 10\%$ , surpassing that of other light-based neuromorphic sensors (Figure 4c). Energy consumption per spike is also estimated by dividing the power consumption of pulses by the number of generated spikes, yielding an approximate 1.5 nJ per spike. This is competitive with that reported in other works (see Figure 4d).<sup>[22,26,34–39]</sup> To further reduce power consumption, we believe device engineering and peripheral circuit design can be employed. It is noteworthy that the linearity is influenced by the operation voltage of the memristor and can be optimized through sensor-memristor co-design (see Figure S11, Supporting Information). More detailed comparison of this work with previous work can be found in Table S2 (Supporting Information). To sum up, our  $\text{NbO}_x$ -based neuromorphic sensor shows outstanding performance in terms of uniformity, energy consumption, and linear encoding, enabling it a competitive candidate for realization of high energy-efficient spike-based VLLS.

To verify the feasibility of the spike-based VLLS in real-world scenarios, we conduct a localization recognition experiment by integrating the SNN for signal processing. The architecture used in the experiment can be found in Figure S12 (Supporting Information). The above results have indicated that the distance between a position and the light source governs the illuminance received by that position, subsequently influencing the spiking behavior. In a pre-designed situation, positions with varying illuminances and distances exhibit distinct spiking features. Through detailed analysis, the illuminance/distance distribution

can be mapped to the distribution of spike frequency, allowing us to infer position information by estimating the spiking frequency, as shown in Figure 5a. For the localization recognition, the SNN serves as a classifier as shown in Figure 5b. Our training dataset consists of 400 samples, while 100 samples are used for testing. The simulation results demonstrate a remarkable accuracy of 97% after 150 epochs, indicating the clear distinction of localization clues (Figure 5c) and the average output and average firing rate during the neural network training is also displayed to verify the results (Figure S13, Supporting Information). The classification of the 100 test datasets are presented in the confusion matrix shown in Figure 5d. The column denotes the position information while the row shows the classification results. The SNN classifier successfully differentiate locations after 150 epochs. Further analysis about the training results, detailed in Figure S14 (Supporting Information), support the conclusion that our spike-based VLLS effectively encodes localization through illuminance and achieves accurate recognition, closely resembling the BSRS. It is worth noting our spike-based VLLS with single neuromorphic sensor is most suitable for indoor scenarios where the illuminance at each point or small area is unique, since the illuminance is the key element that determines the spiking behavior of VLLS. Such requirements, to some extent, limit the application of the spike-based VLLS because current design involves only single neuromorphic sensor. It can be envisioned that, by employing neuromorphic sensor array with outstanding performance, coupling with other sensors,

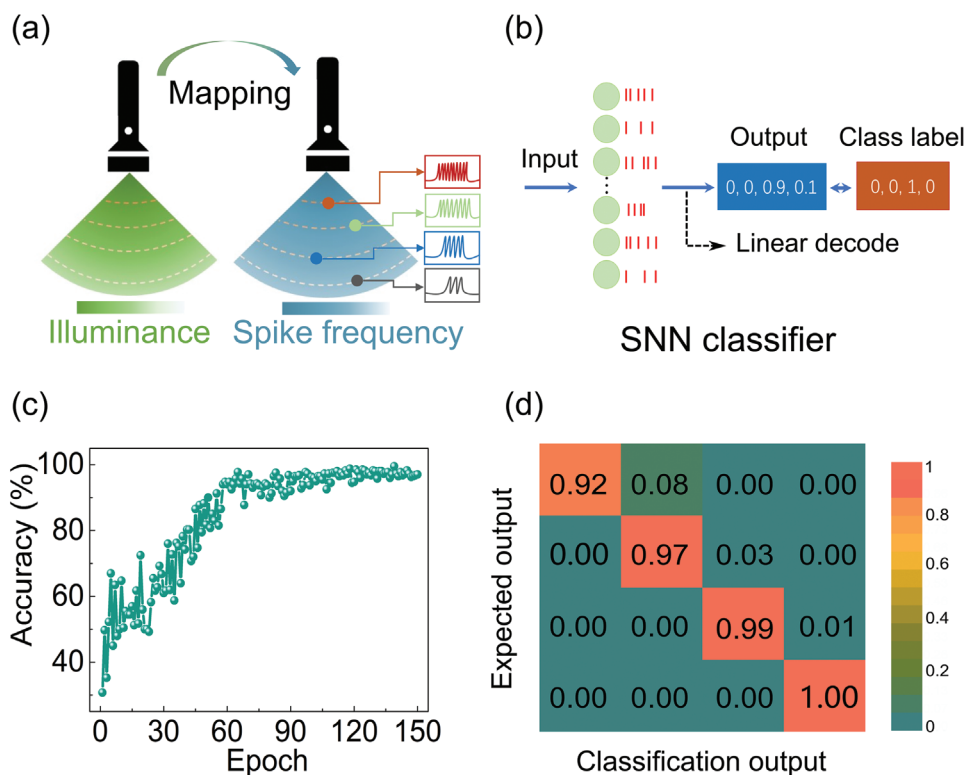


**Figure 5.** Localization classification with spiking-based VLLS. a) Schematic of 4 positions under green light source for data collection. b) The spiking signals represent 4 positions were fed into the SNN which composes of a linear mapping to map 25-dimensional firing rate patterns of spiking neurons to 4-dimensional class labels and implement the classification. c) Evolution of testing accuracy with epochs. After 150 training epochs, the testing accuracy reaches 97%. d) Confusion matrix of simulated classification output versus expected output. The classification result after 150 epoch shows that the positions can be well recognized.

designing, and optimizing the positioning algorithm and peripheral circuit, a more powerful neuromorphic sensor system can be implemented and applied for complicated environment positioning. In brief, our work offers a conceptual and preliminary validation to achieve the positioning in a neuromorphic manner via emerging device, but more efforts are exceedingly required to promote the development of neuromorphic positioning system.

### 3. Conclusion

In summary, a bio-inspired VLLS is reported for precise indoor positioning by integrating an optical neuromorphic sensor and SNN classifier. The optical neuromorphic sensor is designed using a TS memristor with high uniformity and stability, combined with a photoresistor. This sensor can perceive light illuminance and encode it via spikes simultaneously, eliminating the need for conventional signal converters. This feature significantly reduces hardware cost and power consumption. Moreover, the spiking performance of optical neuromorphic sensor is highly dependent on illuminance or the distance between the light source and its position. This property enables the representation of location through spike frequency, making the system suitable for accurate indoor positioning. Importantly, the optical neuromorphic sensor offers additional advantages, such as high uniformity, high linearity, and high sensitivity. To enable precise positioning, the system employs an SNN classifier, which effectively dis-

criminate between four different positions under monochromatic green light. After 150 epochs, it achieves an accuracy of 97%. The spike-based VLLS is highly compact, scalable, and energy-efficient, opening a new avenue for the future development of indoor location systems and positioning technology.

### 4. Experimental Section

**Fabrication of  $\text{NbO}_x$  Volatile Memristor and Electrical Measurement:** The photo lithography and life-off process were used for the patterning. An adhesion layer Ti with a thickness of 5 nm was firstly deposited on the Si/SiO<sub>2</sub> substrate. Then, 30 nm Pt layer bottom electrode was fabricated, followed by the deposition of  $\text{NbO}_x$  dielectric layer. The  $\text{NbO}_x$  was obtained through reactive sputtering with a total gas pressure of 20 mTorr. Finally, 30 nm Pt top electrode was sputtered. All the electrical testing were performed using Agilent B1500A semiconductor parameter analyzer. The photodetector was purchased commercially.

**Materials Characterization:** The sample was first prepared by focused ion beam (FIB) technique with a dual-beam system (Zeiss). Before that, a Pt protective layer was fabricated to avoid any damage during the cutting treatment. Then, the sample was transferred to TEM system (Hitachi-S5500) for elemental analysis such as imaging, elemental mapping, and line scanning.

**Training of the Spiking Neural Network (SNN):** A spiking neural network was designed to classify places with the inputs of spiking train generated by the light memristor device. It composes of a linear mapping to map 25D firing rate patterns of spiking neurons to 4D class labels. The spiking neuron is implemented based on the leaky integrate and fire (LIF)

model. All neurons are fully connected. The backpropagation algorithm was used to train and update the connection weights. The loss function was implemented based on the mean squared error (MSE).

## Supporting Information

Supporting Information is available from the Wiley Online Library or from the author.

## Acknowledgements

This work was supported by the Key-Area Research and Development Program of Guangdong Province (Grants No. 2021B0909060002), National Natural Science Foundation of China (Grants No. 62204219, 62204140), Major Program of Natural Science Foundation of Zhejiang Province (Grants No. LDT23F0401).

## Conflict of Interest

The authors declare no conflict of interest.

## Data Availability Statement

The data that support the findings of this study are available from the corresponding author upon reasonable request.

## Keywords

illumination encoding, indoor visible light localization system, optical neuromorphic sensor, threshold switching memristor

Received: December 28, 2023  
Published online: February 18, 2024

- [1] A. Yassin, Y. Nasser, M. Awad, A. Al-Dubai, R. Liu, C. Yuen, R. Raulefs, E. Aboutanios, *IEEE Commun. Surv. Tutor.* **2017**, *19*, 1327.
- [2] F. Zafari, A. Gkelias, K. K. Leung, *IEEE Commun. Surv. Tutor.* **2019**, *21*, 2568.
- [3] H. Obeidat, W. Shuaieb, O. Obeidat, *Wireless Pers Commun* **2021**, *119*, 289.
- [4] Z. Farid, R. Nordin, M. Ismail, *J. of Computer Networks and Comm.* **2013**, *2013*, 185138.
- [5] F. Alhomayani, M. H. Mahoor, *J. Locat. Based Serv.* **2020**, *14*, 129.
- [6] Y. Chen, W. Guan, J. Li, H. Song, *IEEE Access* **2020**, *8*, 13875.
- [7] A. B. M. M. Rahman, T. Li, Y. Wang, *Sensors* **2020**, *20*, 1382.
- [8] J. Luo, L. Fan, H. Li, *IEEE Commun. Surv. Tutor.* **2017**, *19*, 2871.
- [9] A. H. A. Bakar, T. Glass, H. Y. Tee, F. Alam, M. Legg, *IEEE Trans Instrum. Meas.* **2021**, *70*, 1.
- [10] K. Roy, A. Jaiswal, P. Panda, *Nature* **2019**, *575*, 607.
- [11] X. Ji, X. Zhao, M. C. Tan, R. Zhao, *Adv. Intelligent Sys.* **2020**, *2*, 1900118.
- [12] E. I. Moser, E. Kropff, M. B. Moser, *Annu. Rev. Neurosci.* **2008**, *31*, 69.
- [13] C. D. Harvey, F. Collman, D. A. Dombeck, D. W. Tank, *Nature* **2009**, *461*, 941.
- [14] R. Hayman, M. A. Verriotis, A. Jovalekic, A. A. Fenton, K. J. Jeffery, *Nat. Neurosci.* **2011**, *14*, 1182.
- [15] W. Fischler-Ruiz, D. G. Clark, N. R. Joshi, V. Devi-Chou, L. Kitch, M. Schnitzer, L. F. Abbott, R. Axel, *Neuron* **2021**, *109*, 4036.
- [16] K. Thurley, *Neuron* **2021**, *109*, 2902.
- [17] S. Leutgeb, J. K. Leutgeb, M. B. Moser, E. I. Moser, *Curr. Opin. Neurobiol.* **2005**, *15*, 738.
- [18] J. K. Han, S. Y. Yun, S. W. Lee, J. M. Yu, Y. K. Choi, *Adv. Funct. Mater.* **2022**, *32*, 2204102.
- [19] F. Li, R. Wang, C. Song, M. Zhao, H. Ren, S. Wang, K. Liang, D. Li, X. Ma, B. Zhu, H. Wang, Y. Hao, *ACS Nano* **2021**, *15*, 16422.
- [20] F. Sun, Q. Lu, S. Feng, T. Zhang, *ACS Nano* **2021**, *15*, 3875.
- [21] J. Zhu, X. Zhang, R. Wang, M. Wang, P. Chen, L. Cheng, Z. Wu, Y. Wang, Q. Liu, M. Liu, *Adv. Mater.* **2022**, *34*, 2200481.
- [22] R. Yuan, Q. Duan, P. J. Tiw, G. Li, Z. Xiao, Z. Jing, K. Yang, C. Liu, C. Ge, R. Huang, Y. Yang, *Nat. Commun.* **2022**, *13*, 3973.
- [23] X. Zhang, Y. Zhuo, Q. Luo, Z. Wu, R. Midya, Z. Wang, W. Song, R. Wang, N. K. Upadhyay, Y. Fang, F. Kiani, M. Rao, Y. Yang, Q. Xia, Q. Liu, M. Liu, J. J. Yang, *Nat. Commun.* **2020**, *11*, 51.
- [24] J. Lee, S. Kim, S. Park, J. Lee, W. Hwang, S. W. Cho, K. Lee, S. M. Kim, T. Seong, C. Park, S. Lee, H. Yi, *Adv. Mater.* **2022**, *34*, 2201608.
- [25] J. Han, M. Kang, J. Jeong, I. Cho, J. Yu, K. Yoon, I. Park, Y. Choi, *Adv. Sci.* **2022**, *9*, 2106017.
- [26] C. Chen, Y. He, H. Mao, L. Zhu, X. Wang, Y. Zhu, Y. Shi, C. Wan, Q. Wan, *Adv. Mater.* **2022**, *34*, 2201895.
- [27] G. Li, S. Liu, L. Wang, R. Zhu, *Sci. Robot.* **2020**, *5*, eabc8134.
- [28] M. Wang, Y. Luo, T. Wang, C. Wan, L. Pan, S. Pan, K. He, A. Neo, X. Chen, *Adv. Mater.* **2021**, *33*, 2003014.
- [29] M. Wang, J. Tu, W. Hwang, T. Wang, Z. Liu, F. Zhang, W. Li, K. He, L. Pan, F. Zhang, X. Feng, Q. Liu, M. Liu, X. Chen, *Adv. Mater.* **2022**, *34*, 2201962.
- [30] J. Vongkulbhisal, B. Chantaramolee, Y. Zhao, W. S. Mohammed, *Microw. Opt. Technol. Lett.* **2012**, *54*, 1218.
- [31] S. Kumar, Z. Wang, N. Davila, N. Kumari, K. J. Norris, X. Huang, J. P. Strachan, D. Vine, A. L. D. Kilcoyne, Y. Nishi, R. S. Williams, *Nat. Commun.* **2017**, *8*, 658.
- [32] S. K. Nandi, S. Li, X. Liu, R. G. Elliman, *Appl. Phys. Lett.* **2017**, *111*, 202901.
- [33] L. Gao, P. Y. Chen, S. Yu, *Appl. Phys. Lett.* **2017**, *111*, 103503.
- [34] Y. Yuan, R. Gao, Q. Wu, S. Fang, X. Bu, Y. Cui, C. Han, L. Hu, X. Li, X. Wang, L. Geng, W. Liu, *ACS Sens.* **2023**.
- [35] J. K. Han, S. Y. Yun, J. M. Yu, S. B. Jeon, Y. K. Choi, *ACS Appl. Mater. Interfaces* **2023**, *15*, 5449.
- [36] X. Wang, C. Chen, L. Zhu, K. Shi, B. Peng, Y. Zhu, H. Mao, H. Long, S. Ke, C. Fu, Y. Zhu, C. Wan, Q. Wan, *Nat. Commun.* **2023**, *14*, 3444.
- [37] Y. Wang, Y. Gong, S. Huang, X. Xing, Z. Lv, J. Wang, J. Q. Yang, G. Zhang, Y. Zhou, S. T. Han, *Nat. Commun.* **2021**, *12*, 5979.
- [38] J. K. Han, D. M. Geum, M. W. Lee, J. M. Yu, S. K. Kim, S. Kim, Y. K. Choi, *Nano Lett.* **2020**, *20*, 8781.
- [39] Q. Wu, B. Dang, C. Lu, G. Xu, G. Yang, J. Wang, X. Chuai, N. Lu, D. Geng, H. Wang, L. Li, *Nano Lett.* **2020**, *20*, 8015.